

1 **Experimental Investigation of CO₂ Buoyant Flow**
2 **Saturation: The Impact of Realistic Bedforms and**
3 **Heterogeneous Wettability**

4 **J. E. Ubillus^{1,2}, H. Ni², D. DiCarlo¹**

5 ¹Hildebrand Department of Petroleum and Geosystems Engineering, The University of Texas at Austin
6 ²Bureau of Economic Geologic, The University of Texas at Austin

7 **Key Points:**

- 8 • Bedform architecture modifications and wettability changes can significantly im-
9 pact nonwetting saturation and capillary heterogeneity trapping.

Corresponding author: Hailun Ni, hailun.ni@beg.utexas.edu

Abstract

We produce realistic sedimentary formations consisting of ripple deposits with varying grain size contrast and wettability in a meter-scale slab chamber. Then, we conduct multiphase flow experiments through these structures and measure the infiltration patterns, capillary heterogeneity trapping, and overall trapping performance. When we alter the ripple bedform architecture, variations in trapped saturation and capillary heterogeneity trapping (10% to 20%) increment are exhibited. Similar growth in trapping performance is also observed when grain size contrast increases. Finally, wettability changes (water- to oil-wet) can increase nonwetting saturation and capillary heterogeneity trapping up to 5% and 10-20%, respectively. These results emphasize the importance of correctly characterizing the impact of small-scale heterogeneities and wettability changes.

Plain Language Summary

We make sediment layers in a 60-cm tank. These layers look like the ones you would find in real Earth formations. Then, we conduct the flow experiment through these layers to see how they affect the fluid movement. We look at how the fluid spread out and get trapped in the layers. Depending on how we arrange the ripples in the layers, we notice that more liquid gets trapped in certain places. Also, when we use grains that are very different in size, we see more liquid getting stuck in the layers. And if we change how much the grains like water or oil, we find that more liquid of one type gets trapped compared to the other. It is important to understand these small differences to study how fluids move through Earth's layers accurately.

1 Introduction

Carbon dioxide (CO₂) geologic storage has become a pivotal strategy for addressing climate change. During this process, CO₂ is captured from various sources, compressed, and transported before being injected into porous media formations capable of securely retaining the supercritical fluid. Deep saline aquifers represent prime targets for CO₂ storage due to their extensive capacity and global ubiquity (Holloway, 2005; IPCC, 2005; Krevor et al., 2023). Importantly, the sedimentary formations harboring these saline aquifers exhibit inherent natural geological heterogeneities (Bachu, 2003; Eikehaug et al., 2024; Flett et al., 2007; Jackson & Krevor, 2020; Krishnamurthy et al., 2022). Previous studies have shown that centimeter-scale heterogeneities can profoundly influence CO₂ migration and trapping dynamics (Davidson et al., 2022; Krishnamurthy et al., 2017; Trevisan et al., 2015). Therefore, conducting experimental investigations is imperative to quantify the impact of such heterogeneities on trapping performance precisely.

Recent studies, including investigations at pore- and core-scale levels (e.g., micro-models, micro-CT imaging, and core flooding), have been influential in unraveling the intricacies of CO₂ fluid behavior within sedimentary rocks (Bakhshian & Hosseini, 2019; Krevor et al., 2011; Krishnamurthy et al., 2017; Kurotori & Pini, 2021; Li & Benson, 2015; Ni et al., 2019; Seyyedi et al., 2022; Trevisan, Gonzalez-Nicolas, et al., 2017; Trevisan, Pini, et al., 2017). However, these studies could only consider the influence of small-scale heterogeneities within their domain sizes, which are limited. In contrast, intermediate tank-scale experiments offer a broader domain size, enabling a more comprehensive characterization of heterogeneity effects. Considerable attention has been devoted to tank-scale experiments to elucidate CO₂ fluid flow dynamics.

For instance, Trevisan et al. (2015) conducted sand tank experiments mimicking an aquifer configuration, demonstrating that dm-scale heterogeneities can increase CO₂ storage capacity through local capillary trapping. In addition, Agartan et al. (2015, 2020) studied the effect of small-scale heterogeneities on dissolution trapping. Their results suggest that dissolved CO₂ remains immobilized below low-permeability zones. Despite the

59 effort to quantify the effect of small-scale heterogeneities through sand tank experiments,
60 such sand configurations do not match realistic sedimentary structures in nature.

61 Subsequent research entailed multiphase flow tank-scale experiments using an au-
62 tomated feeder machine to replicate realistic heterogeneous conditions. Such tank-scale
63 experimental methods are valuable as they allow engineering of different degrees and types
64 of heterogeneity present in nature. Krishnamurthy et al. (2022) underscored that increased
65 grain size contrast (i.e., degree of heterogeneity) correlates with a higher buoyant flow
66 nonwetting saturation level on cross-bedded formations. Other than cross-beds and her-
67 ringbone structures (Davidson et al., 2022), no other studies have been conducted on dif-
68 ferent types of sedimentary domains. However, Ni et al. (2023) demonstrated that het-
69 erogeneity geometry can significantly impact the amount of CO₂ capillary trapping. There-
70 fore, in this work, we look at different realistic ripple domains to quantify how variations
71 in bedform patterns affect trapping.

72 In adjacent research in oil recovery, studies have found that wettability profoundly
73 influences fluid flow dynamics (Masalmeh, 2003; Spiteri et al., 2008). Most sedimentary
74 rocks in deep saline aquifers, notably sandstones, typically exhibit high water-wet char-
75 acteristics. Nevertheless, these reservoirs may exhibit variability in wettability, which can
76 subsequently impact fluid migration and trapping behaviors (Al-Khdheawi et al., 2017).
77 Numerous studies have explored pore-scale homogeneous domains to quantify changes
78 in saturation and trapping using techniques such as micro-CT imaging (Celauro et al.,
79 2014; Geistlinger & Ataei-Dadavi, 2015). However, the scientific literature needs more
80 investigations into tank-scale wettability alterations across various types of heterogeneities.

81 In this study, we assess the impact of modifications in bedform architecture, vari-
82 ations on grain size contrast, and wettability changes in ripple bedforms on trapping per-
83 formance. Here, we perform capillary- and buoyancy-driven flow experiments within a
84 3D slab and capture the migration patterns using light transmission techniques. In the
85 following sections, we discuss the fluid flow dynamics regarding ripple domains and the
86 effect of the degree of heterogeneity and wettability on trapped saturation. Addition-
87 ally, we explored the implications of such variations on capillary heterogeneity trapping.

88 2 Experimental Overview

89 Realistic heterogeneities found in nature are selected from Rubin and Carter (2006)
90 bedform architecture models. For this study, we choose ripple patterns consisting of two
91 different facies: matrix (coarse grains) and laminae (fine grains). The patterns are packed
92 using glass beads of different diameters with an automated feeding system in a 3D slab
93 chamber (60 x 60 x 2 cm³) (Krishnamurthy et al., 2019). The height of the heteroge-
94 neous portion of the domain is approximately 42 cm.

95 Glass beads with varying degrees of wettability are used. The wettability of the
96 glass beads was estimated by measuring the contact angle between the beads and wa-
97 ter (Guo et al., 2023; Hernandez, 2011; Wang & Tokunaga, 2015).

98 The multiphase flow experiments consist of drainage and redistribution, with both
99 stages at atmospheric conditions with inlet constant rate and outlet constant pressure.
100 Heptane (i.e., nonwetting phase) (S_{nw}) and a glycerol-water mixture (i.e., wetting phase)
101 are used as analog fluids for supercritical CO₂ and in-situ brine, respectively (Krishnamurthy
102 et al., 2019; Ni & Meckel, 2021). To prepare for the experiment, the chamber is filled with
103 the glycerol-water mixture at high flow rates to dissolve gaseous CO₂, previously injected
104 to displace air inside the tank, until the mixture flows out from the outlet reservoir.

105 During the drainage phase, heptane is injected from the bottom middle inlet of the
106 chamber at a low flow rate (0.2 ml/min) to guarantee that the flow is gravity- and capillary-
107 driven. The injection continues for 24 hours after heptane leaves the chamber. Redis-

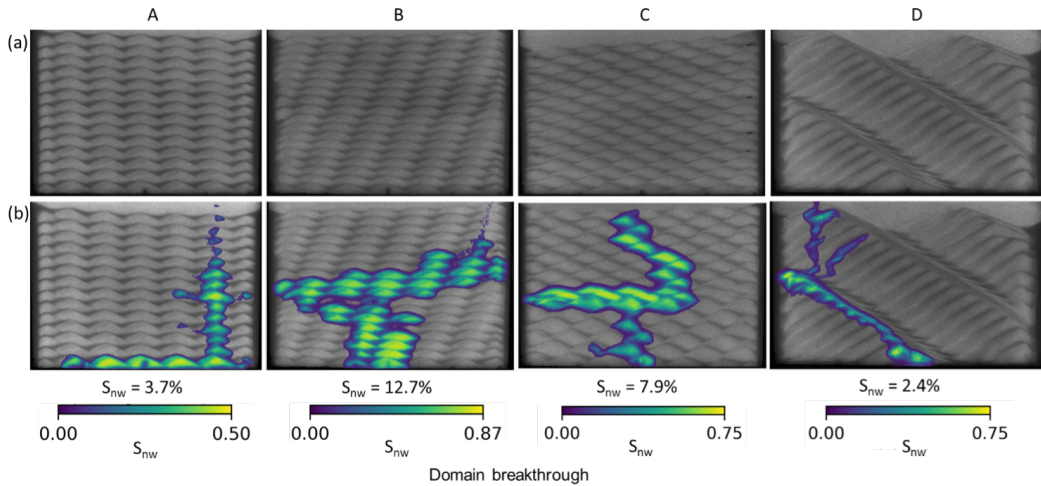


Figure 1. Figure 1. (a) Ripple domain patterns with slight changes in the ripple crest phase. A: in-phase, B: slightly out-of-phase, C: out-of-phase, and D: large out-of-phase. (b) Break-through nonwetting phase saturation field and domain average saturation values for all patterns. The color bar shows pixel-wise nonwetting saturation.

108 tribution happens immediately after stopping the injection and lasts for 24 hours. A light
 109 transmission visualization technique (Bob et al., 2008; Darnault et al., 1998; DiCarlo,
 110 2004; Krishnamurthy et al., 2022; Niemet et al., 2002; Tidwell & Glass, 1994; Weisbrod
 111 et al., 2003) is used throughout the entire experiment to capture the nonwetting phase
 112 saturation. Saturation fields are recorded every 30 seconds for the drainage stage and
 113 every 30 minutes for the redistribution stage. We report three saturation fields taken through-
 114 out the experiment: at heterogeneous domain breakthrough, the end of injection (drainage),
 115 and the end of redistribution.

116 We conduct three sets of experiments in the study. Firstly, different ripple bedform
 117 architectures are packed (in-phase, slightly out-of-phase (i.e., climbing), out-of-phase, and
 118 large climbing ripples) with constant grain size contrast between the matrix and the lam-
 119 inae facies. Secondly, in-phase ripples with varying grain size contrast are filled to val-
 120 idate previously obtained results on a cross-laminated bedform architecture (Krishnamurthy
 121 et al., 2022). Thirdly, ripple bedforms architecture with constant grain size contrast and
 122 different wettability (water- to oil-wet).

123 3 Results

124 3.1 Changes in bedform architecture

125 Figure 1a shows the four ripple patterns (A to D) that we used – there are slight
 126 modifications on the ripple crest phases between layers, and Experiment D also shows
 127 an increase in ripple size. Figure 1b shows the 2D nonwetting phase saturation for each
 128 bedform at breakthrough. We observe that a slight displacement in ripple phases allowed
 129 the nonwetting phase to extend farther laterally and accumulate in more layers. The com-
 130 bined effect increases the nonwetting phase saturation in the heterogeneous domain and
 131 changes the migration pattern from fingering to more capillary heterogeneity trapping
 132 behind capillary barriers.

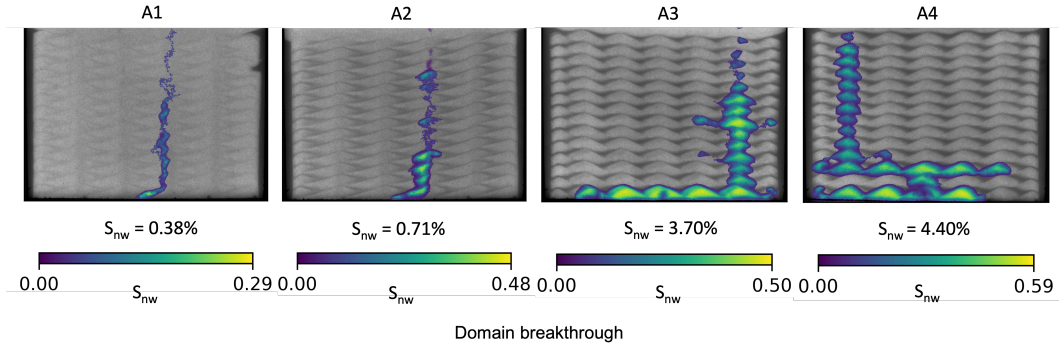


Figure 2. Figure 2. Nonwetting phase saturation field and domain average saturation values at breakthrough for in-phase ripples with increasing degree of heterogeneity (A1 to A4). The color bar shows pixel-wise nonwetting saturation.

133

3.2 Changes in grain size contrast

134

135

136

137

138

139

140

141

142

In addition to the multiple ripple bedform architectures, experiments with varying grain size contrast for the in-phase ripple pattern were performed. Figure 2 shows the breakthrough nonwetting saturation field with grain size contrast increasing from A1 to A4. When the size contrast between the coarse and fine grains is small (A1 and A2), the nonwetting phase fluid breaks through the domain as a finger quickly. At higher contrast (A3 and A4), the fluid builds up column height beneath the laminae and extends laterally until a zone of low capillary entry pressure is reached to move up into the upper layers. Increasing grain size contrast leads to more nonwetting phase saturation trapped within the heterogeneous domain.

143

3.3 Changes in wettability

144

145

146

147

148

149

150

151

152

153

Besides conducting experiments on the type and degree of heterogeneity, we ran experiments in ripple patterns to study the effect of wettability on nonwetting phase saturation. Glass beads with variations in contact angle were selected. Note that only the wettability of the matrix (coarse) changed, while the laminae (fine) remained water-wet for all experiments. The domain and grain size contrast were also kept constant. Water- and intermediate-wet experiments were filled entirely by the wetting phase. However, during water injection, the oil-wet scenarios had gas bubbles trapped within the domain because of the affinity of the beads to retain gas during experiment preparation. Figure 3 shows the nonwetting phase saturation at breakthrough for in-phase and out-of-phase ripples with different contact angles.

154

3.4 Total trapped saturation

155

156

157

158

159

160

161

162

Although we measure the saturation field throughout each experiment, here, we summarize the total trapped saturation at the end of drainage. This is slightly higher than the breakthrough saturation as new migration pathways are formed during the drainage stage, which leads to more fluid accumulation pools. Figure 4 shows drainage saturations as a function of the type of heterogeneity, degree of heterogeneity, and contact angle. The dimensionless parameter δ is used to capture the degree of heterogeneity of the bedforms and is a function of the mean and standard deviation of the matrix and laminae (Krishnamurthy et al., 2022).

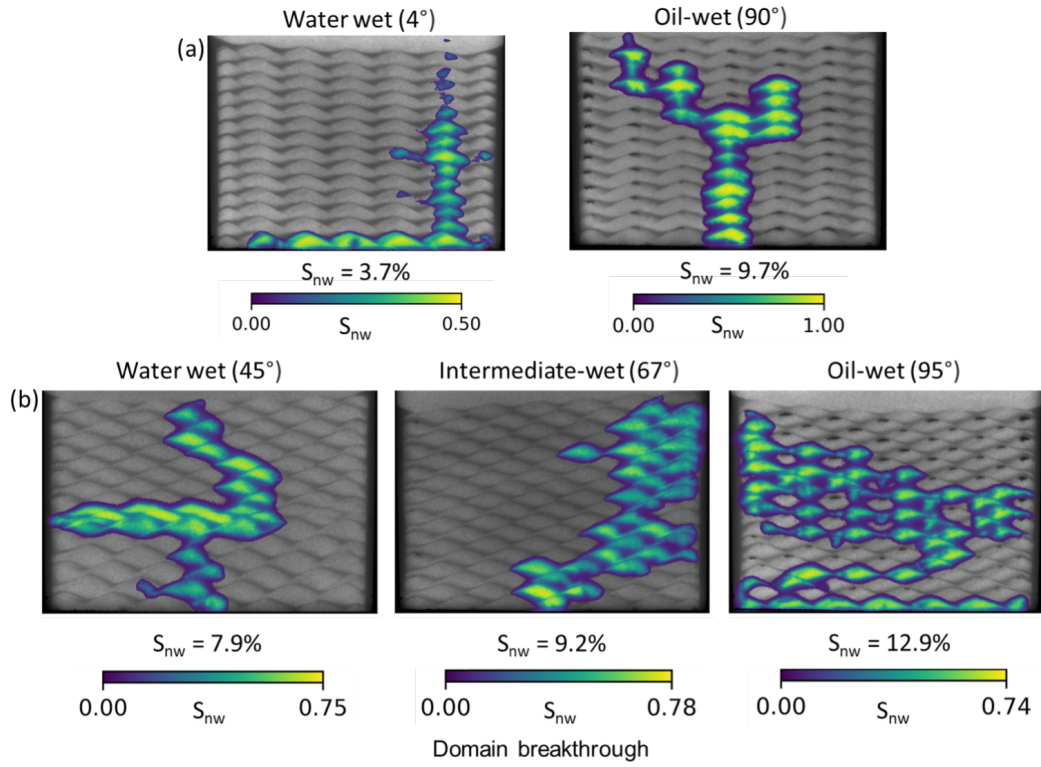


Figure 3. Figure 3. Heptane (representing supercritical CO_2) saturation field and domain average saturation values at breakthrough for in-phase (a) and out-of-phase (b) ripples with varying wettability. The color bar shows pixel-wise nonwetting saturation.

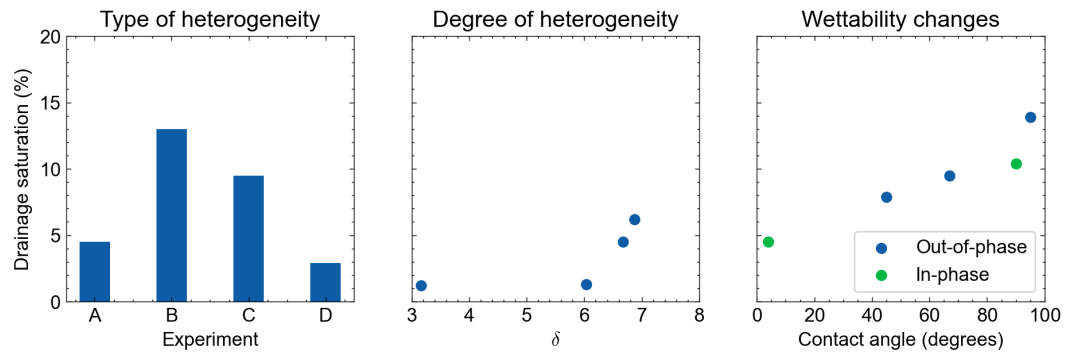


Figure 4. Figure 4. Domain average drainage saturation versus type of heterogeneity, degree of heterogeneity, and contact angle.

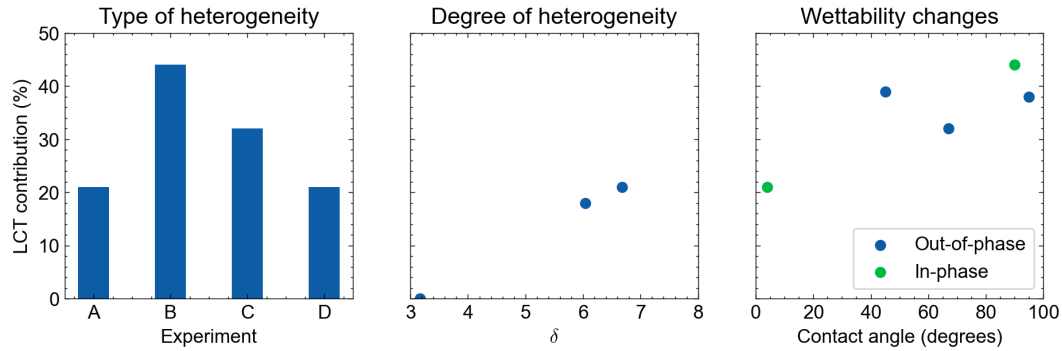


Figure 5. Figure 5. Contribution of CHT to total trapping as a function of the type of heterogeneity, degree of heterogeneity, and contact angle.

163

3.5 Capillary heterogeneity trapping

164

165

166

167

168

169

170

171

172

After the redistribution stage, some regions below capillary barriers exhibit a saturation greater than residual. This excess saturation is known as local capillary trapping or capillary heterogeneity trapping (CHT). Residual saturation for homogeneous water-wet glass beads can be assumed to be within the range of 0.16–0.25 (Chatzis et al., 1983; Dullien et al., 1989; Mayer & Miller, 1992). The CHT contribution was computed as the average pixel-level ratio of the difference between redistribution and residual saturation (assumed 0.25) over redistribution saturation (Krishnamurthy et al., 2022). Figure 5 shows the percentage contribution of CHT to total trapping as a function of the type of heterogeneity, degree of heterogeneity, and contact angle.

173

4 Discussion

174

175

In this and the following subsections, we analyze the results further and discuss potential reasons for and implications of our observations.

176

4.1 Fluid flow dynamics in ripple bedforms

177

178

179

180

181

182

183

184

We observe that the phase of the ripples (patterns A through C) changes the amount of trapped saturation after drainage and redistribution. To understand why, we first describe the dynamics of the ripples that were created. When ripples are built by the automated feeder apparatus, beads will tend to roll down from the crest to the trough because of gravity. Therefore, a thinner laminae barrier is produced at the crest, potentially leaving gaps in the fine media and a lower capillary entry pressure. The latter can be observed in Figure 1a, where the sides of the ripples show a darker color compared to the crest. This dark color is a consequence of fine bead accumulation.

185

186

187

188

189

In the case of in-phase ripples (A), all the ripple crests will be aligned on top of each other. The fluid moves laterally during injection until it builds sufficient column height to percolate to the upper layer. Generally, for in-phase ripples, the fluid will migrate following a preferential flow pathway through the similar crest location in all layers, thus leading to a low breakthrough and drainage nonwetting saturation.

190

191

192

193

194

On the other hand, out-of-phase ripples can be slightly or entirely unaligned, meaning that crests will tend to be aligned with troughs, creating potentially high capillary entry pressure barriers that increase breakthrough and drainage nonwetting saturation. Nonetheless, there is no trend for how crest phase-shifting influences saturation as slightly out-of-phase ripples (B) present higher nonwetting saturation than completely out-of-

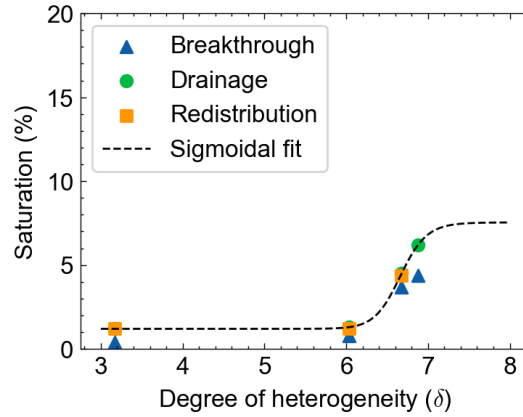


Figure 6. Figure 6. Overall nonwetting phase saturation after each experiment stage as a function of the degree of heterogeneity. The dashed line represents the S-shaped curve fitted to the drainage saturation, as Krishnamurthy et al. (2022) demonstrated.

195 phase (C). In the case of large climbing ripples (D), the sides of the crests are aligned
 196 in each layer, building a thicker diagonal lamination with high capillary entry pressure.
 197 Once the fluid reaches the lamination, it preferentially flows underneath such barriers
 198 until it migrates to the adjacent ripple layer.

199 As a result, various ripple patterns will exhibit different breakthrough and drainage
 200 nonwetting saturation (Figure 4). Such flow dynamics behavior will also have implica-
 201 tions on CHT. Slight changes in ripple bedform can increment 10 to 20% the contribu-
 202 tion of CHT, as shown in Figure 5.

203 4.2 The effect of the grain size contrast in ripple bedforms

204 Previously, Krishnamurthy et al. (2022) demonstrated that an increase in grain size
 205 contrast leads to a higher nonwetting phase saturation when measured in cross-bedded
 206 heterogeneities. Saturation increases until it reaches a plateau at a higher degree of het-
 207 erogeneity. This behavior in saturation can be modeled as a sigmoidal S-shaped curve
 208 as a function of the dimensionless parameter δ (function of the mean and standard de-
 209 viation of the matrix and laminae). We apply the same analysis to in-phase ripple do-
 210 mains measured here, and we find similar behavior. Figure 6 displays the domain aver-
 211 age nonwetting saturation at each experiment stage as a function of the degree of het-
 212 erogeneity. For this bedform architecture, nonwetting phase saturation increases until
 213 it reaches a plateau of approximately 8%. Further, an increase in the degree of hetero-
 214 geneity will increase CHT contribution until a plateau of 20% is reached at higher de-
 215 gree contrasts (Figure 5).

216 Both saturation and CHT plateaus differ from cross-bedded formation values (34%
 217 and 80%, respectively). These results suggest that the structural complexity of the het-
 218 erogeneity controls the plateau, as saturation and CHT differ from one bedform archi-
 219 tecture to another.

220 4.3 The effect of wettability changes in ripple bedforms

221 In addition to the type and degree of heterogeneity, wettability alterations can also
 222 impact the trapped saturation within the heterogeneous domain. These alterations in
 223 wettability promote lateral migration and discourage vertical displacement in ripple bed-

224 forms, as shown in Figure 3. Thus, it increases the domain sweep efficiency, hence, the
 225 overall saturation.

226 Ripple bedforms show a monotonic relation between contact angle and saturation
 227 (Figure 4). As a result, an increase of approximately 5% in drainage saturation when
 228 shifting from water- to oil-wet beads is observed. Nevertheless, during water injection,
 229 oil-wet scenarios (Figure 3) have gas bubbles trapped inside the domain because of the
 230 tendency of the beads to retain gas. The presence of the bubbles will reduce nonwetting
 231 saturation because (a) gas will reduce the pore space available to the nonwetting phase
 232 as it migrates, and (b) gas will decrease the necessary nonwetting phase column height
 233 to overcome the capillary entry pressure of the beads because the gas column itself has
 234 a higher buoyancy force. The latter suggests that more nonwetting phase saturation can
 235 be achieved in oil-wet ripples.

236 Such monotonic behavior is also exhibited in the contribution of CHT to total trap-
 237 ping (Figure 5). However, this trend can be significantly modified by the type of het-
 238 erogeneity variations. In the case of in-phase ripples, as the water-wet domain shifts to
 239 oil-wet, the contribution of CHT increases by approximately 20%. On the other hand,
 240 CHT contribution on out-of-phase ripples, independent of contact angle, remains close
 241 to 40%.

242 4.4 Trapping efficiency: Initial-Residual scatter plots

243 During the redistribution stage under hydrostatic conditions, we observe that the
 244 nonwetting phase escapes the domain, decreasing saturation. However, most of the fluid
 245 remains trapped inside the domain. Thus, the trapped nonwetting phase is highly cor-
 246 related with the drainage saturation. To evaluate the trapping performance, we plot Ini-
 247 tial – Residual (IR) plots, which are commonly used to generate parametric trapping mod-
 248 els (Krevor et al., 2015; Krishnamurthy et al., 2022; Ni et al., 2019; Spiteri et al., 2008).
 249 Our slab-scale experiment allows us to plot this on a pixel-by-pixel basis. Figure 7 shows
 250 the pixel-level redistribution saturation as a function of the drainage saturation for the
 251 type of heterogeneity (a), degree of heterogeneity (b), and wettability changes (c). More-
 252 over, the ratio between redistribution and drainage average saturation was estimated to
 253 quantify the domain trapping efficiency percentage (shown in parenthesis). Finally, the
 254 Land trapping model was fitted to all experimental results. Land coefficient (C) equal
 255 to zero (i.e., 100% efficiency) represents that the nonwetting phase remains trapped af-
 256 ter redistribution. Therefore, higher values of C indicate worse trapping performance.
 257 Experiment A4 lacks redistribution saturation and thus is excluded from this analysis.

258 4.5 Impact of type and degree of heterogeneity, and wettability changes 259 on trapping performance

260 The scatter shape of the IR plots differs between ripple patterns, as shown in Fig-
 261 ure 7a. This observation suggests an interplay between domain heterogeneity type and
 262 trapping performance. In the ripple pattern case, a slight shift in the crest leads to a de-
 263 crease in trapping efficiency. When the amount of scatter increases above the 100% trap-
 264 ping line ($C=0$), a high trapping efficiency is expected, as the fluid redistributes within
 265 the domain and remains trapped. Conversely, a low trapping efficiency is expected for
 266 domains with increasing scatter below the 100% trapping line, where the nonwetting phase
 267 redistributes and escapes the domain.

268 Figure 7b shows that an increase in the degree of heterogeneity provokes a higher
 269 amount of scatter, which leads to variation in trapping performance. Changes in the de-
 270 gree of heterogeneity do not show a concrete trend in trapping efficiency. Since the amount
 271 of scatter is balanced on both sides of the 100% trapping line, this explains why in-phase
 272 ripples, independent of grain size contrast, will exhibit trapping efficiencies above 90%.

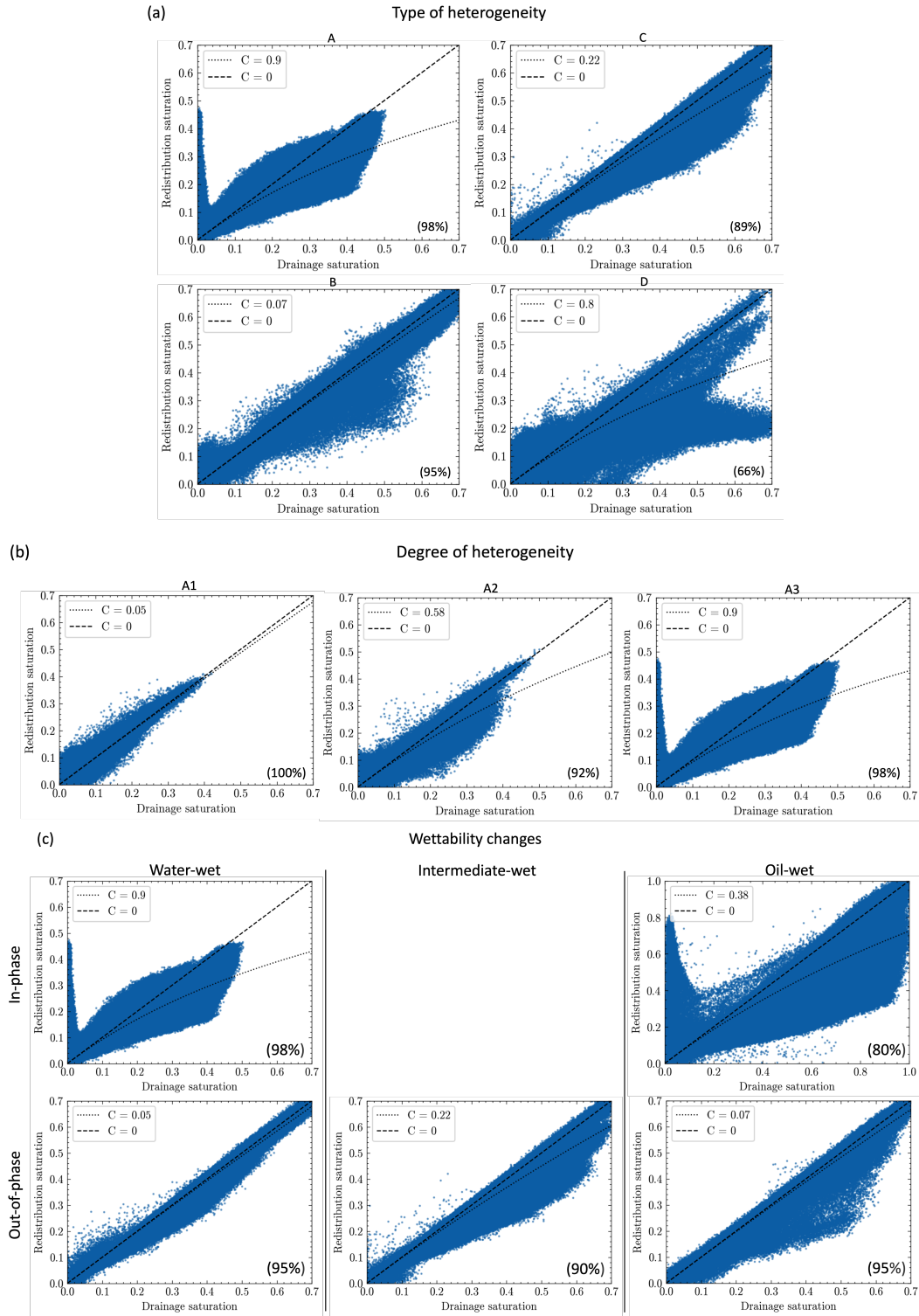


Figure 7. Figure 7. Pixel-wise redistribution nonwetting saturation as a function of drainage saturation for the type of heterogeneity (a), degree of heterogeneity (b), and wettability (c). The dashed line shows 100% trapping ($C=0$), and the dotted line depicts the domain average Land trapping coefficient. Values in parenthesis represent the trapping efficiency as the overall redistribution and drainage saturation ratio.

273 An increase in fitted C is expected as a high degree of heterogeneity allows for more fluid
274 redistribution (Krishnamurthy et al., 2022).

275 However, more care should be taken when using the Land trapping model to de-
276 fine trapping performance. A higher domain C value can indicate nonwetting phase re-
277 distributing within the domain (i.e., higher CHT contribution). Thus, a considerable CHT
278 contribution can significantly impact the Land trapping model as the model is designed
279 to fit pore-scale residual trapping data better.

280 Finally, we observed in Figure 7c that the scatter shape of the IR plots remains con-
281 stant when the type and degree of heterogeneity are unaltered. However, the amount of
282 scatter increment in the IR plots is because of the domain matrix wettability variation
283 from water to oil-wet. The previous observations demonstrate that the trapping perfor-
284 mance of the domain is highly correlated with the domain wettability. Fitted domain
285 C values do not consider the heterogeneous wettability throughout the domain (assumed
286 homogeneous), which can lead to an inaccurate Land trapping coefficient.

287 5 Summary and Conclusions

288 In this study, we conduct tank-scale multiphase flow experiments in various rip-
289 ple pattern domains with variations in grain size contrast and domain matrix wettabil-
290 ity to quantify their effects on saturation, capillary heterogeneity trapping, and overall
291 trapping performance. We demonstrate that slight changes in bedform architecture can
292 significantly impact nonwetting saturation. Moreover, we found that capillary hetero-
293 geneity trapping is highly dependent on the type of heterogeneity, as subtle changes in
294 ripple patterns can increment CHT by 10 – 20%. Additionally, we have corroborated that
295 an increase in grain size contrast between matrix and laminae increases nonwetting sat-
296 uration, as Krishnamurthy et al. (2022) proposed for cross-bedded formations. We val-
297 idated that an increase in the contribution of CHT is expected at higher degree contrasts.
298 Finally, our findings on wettability changes on the domain matrix facies suggest that with
299 a shift from water- to oil-wet grains, a 5% increase in nonwetting saturation can be achieved,
300 and an increment of 10% to 20% on CHT contribution can be expected.

301 Open Research Section

302 The experimental data in the study are available at UT-Austin Dataverse via [https://
303 dataverse.tdl.org/dataverse/ripplebedform](https://dataverse.tdl.org/dataverse/ripplebedform)

304 Disclaimer

305 This report was prepared as an account of work sponsored by an agency of the United
306 States Government. Neither the United States Government nor any agency thereof, nor
307 any of their employees, makes any warranty, express or implied, or assumes any legal li-
308 ability or responsibility for the accuracy, completeness, or usefulness of any information,
309 apparatus, product, or process disclosed, or represents that its use would not infringe
310 privately owned rights. Reference herein to any specific commercial product, process, or
311 service by trade name, trademark, manufacturer, or otherwise does not necessarily con-
312 stitute or imply its endorsement, recommendation, or favoring by the United States Gov-
313 ernment or any agency thereof. The views and opinions of authors expressed herein do
314 not necessarily state or reflect those of the United States Government or any agency thereof.

315 Acknowledgments

316 This work was supported by the Energy Institute at The University of Texas at Austin
317 through the Energy Seed Grant and by the U.S. Department of Energy through the Gulf
318 of Mexico Partnership for Offshore Carbon Storage under grant award number DE-FE0031558.

319 Special thanks to Mason Fleming for his splendid work during his Summer Research In-
 320 ternship Experience (SURI) funded by the Hildebrand Department of Petroleum and Geosys-
 321 tems Engineering at The University of Texas at Austin.

322 References

- 323 Agartan, E., Illangasekare, T. H., Vargas-Johnson, J., Cihan, A., & Birkholzer, J.
 324 (2020). Experimental investigation of assessment of the contribution of hetero-
 325 geneous semi-confining shale layers on mixing and trapping of dissolved CO_2 in
 326 deep geologic formations. *International Journal of Greenhouse Gas Control*,
 327 *93*. doi: <https://doi.org/10.1016/j.ijggc.2019.102888>
- 328 Agartan, E., Trevisan, L., Cihan, A., Birkholzer, J., Zhou, Q., & Illangasekare, T. H.
 329 (2015). Experimental study on effects of geologic heterogeneity in enhancing
 330 dissolution trapping of supercritical CO_2 . *Water Resources Research*, 1635-1648.
 331 doi: <https://doi.org/10.1002/2014WR015778>
- 332 Al-Khdheawi, E. A., Vialle, S., Barifcani, A., Sarmadivaleh, M., & Iglauer, S.
 333 (2017). Impact of reservoir wettability and heterogeneity on CO_2 plume migra-
 334 tion and trapping capacity. *International Journal of Greenhouse Gas Control*,
 335 *58*, 142-158. doi: <http://dx.doi.org/10.1016/j.ijggc.2017.01.012>
- 336 Bachu, S. (2003, 6). Screening and ranking of sedimentary basins for sequestration
 337 of CO_2 in geological media in response to climate change. *Environmental Geol-*
 338 *ogy*, *44*, 277-289. doi: 10.1007/s00254-003-0762-9
- 339 Bakhshian, S., & Hosseini, S. A. (2019, 4). Pore-scale analysis of supercritical
 340 CO_2 -brine immiscible displacement under fractional-wettability conditions. *Ad-*
 341 *vances in Water Resources*, *126*, 96-107. doi: 10.1016/J.ADVWATRES.2019
 342 .02.008
- 343 Bob, M. M., Brooks, M. C., Mravik, S. C., & Wood, A. L. (2008, 5). A modi-
 344 fied light transmission visualization method for dnapi saturation measure-
 345 ments in 2-d models. *Advances in Water Resources*, *31*, 727-742. doi:
 346 10.1016/j.advwatres.2008.01.016
- 347 Celauro, J. G., Torrealba, V. A., Karpyn, Z. T., Klise, K. A., & Mckenna, S. A.
 348 (2014, 2). Pore-scale multiphase flow experiments in bead packs of variable
 349 wettability. *Geofluids*, *14*, 95-105. doi: 10.1111/gfl.12045
- 350 Chatzis, J., Morrow, N., & Lim, H. (1983). Magnitude and detailed structure of
 351 residual oil saturation. *SPE Journal*, *23*, 311-326. doi: [https://doi.org/10](https://doi.org/10.2118/10681-PA)
 352 .2118/10681-PA
- 353 Darnault, C. J., Throop, J. A., Dicarolo, D. A., Rimmer, A., Steenhuis, T. S., & Par-
 354 lange, J. Y. (1998, 6). Visualization by light transmission of oil and water
 355 contents in transient two-phase flow fields. *Journal of Contaminant Hydrology*,
 356 *31*, 337-348. doi: 10.1016/S0169-7722(97)00068-5
- 357 Davidson, M. A., Mumford, K. G., Mullins, N., & Calvert, M. M. (2022). Modifi-
 358 cation of a 3d printer to create geologically realistic heterogeneous sand packs.
 359 *Vadose Zone Journal*. doi: 10.1002/vzj2.20216
- 360 DiCarlo, D. A. (2004). Experimental measurements of saturation overshoot on infil-
 361 tration. *Water Resources Research*, *40*. doi: 10.1029/2003WR002670
- 362 Dullien, F. A. L., Zarcone, C., Macdonald, I. F., Collins, A., & Bochard, R. D. E.
 363 (1989). The effects of surface roughness on the capillary pressure curves
 364 and the heights of capillary rise in glass bead packs. *Journal of Col-*
 365 *loid and Interface Science*, *127*, 362-372. doi: [https://doi.org/10.1016/](https://doi.org/10.1016/0021-9797(89)90042-8)
 366 0021-9797(89)90042-8
- 367 Eikehaug, K., Haugen, M., Folkvord, O., Benali, B., Larsen, E. B., Tinkova, A., ...
 368 Fernø, M. A. (2024). Engineering meter-scale porous media flow experiments
 369 for quantitative studies of geological carbon sequestration. *Transport in Porous*
 370 *Media*. doi: 10.1007/s11242-023-02025-0
- 371 Flett, M., Gurton, R., & Weir, G. (2007, 5). Heterogeneous saline formations for

- 372 carbon dioxide disposal: Impact of varying heterogeneity on containment and
 373 trapping. *Journal of Petroleum Science and Engineering*, 57, 106-118. doi:
 374 10.1016/j.petrol.2006.08.016
- 375 Geistlinger, H., & Ataei-Dadavi, I. (2015). Influence of the heterogeneous wettability
 376 on capillary trapping in glass-beads monolayers: Comparison between
 377 experiments and the invasion percolation theory. *Journal of Colloid and In-*
 378 *terface Science*, 459, 230-240. Retrieved from [http://dx.doi.org/10.1016/](http://dx.doi.org/10.1016/j.jcis.2015.07.074)
 379 [j.jcis.2015.07.074](http://dx.doi.org/10.1016/j.jcis.2015.07.074) doi: 10.1016/j.jcis.2015.07.074
- 380 Guo, Y., Shi, Y., & Mohanty, K. (2023). Improvement of polymer flooding of a vis-
 381 cous oil by addition of an alkali.. doi: <https://doi.org/10.2118/215108-MS>
- 382 Hernandez, A. (2011). *Observations of buoyant plumes in countercurrent displace-*
 383 *ment*. The University of Texas at Austin.
- 384 Holloway, S. (2005). Underground sequestration of carbon dioxide-a viable green-
 385 house gas mitigation option. *Energy*, 30, 2318-2333. doi: 10.1016/j.energy.2003
 386 .10.023
- 387 IPCC. (2005). *Special report on carbon dioxide capture and storage* (Tech. Rep.).
- 388 Jackson, S. J., & Krevor, S. (2020, 9). Small-scale capillary heterogeneity linked to
 389 rapid plume migration during co2 storage. *Geophysical Research Letters*, 47.
 390 doi: 10.1029/2020GL088616
- 391 Krevor, S., Blunt, M. J., Benson, S. M., Pentland, C. H., Reynolds, C., Al-Menhali,
 392 A., & Niu, B. (2015, 1). Capillary trapping for geologic carbon dioxide storage
 393 - from pore scale physics to field scale implications. *International Journal of*
 394 *Greenhouse Gas Control*, 40, 221-237. doi: 10.1016/j.ijggc.2015.04.006
- 395 Krevor, S., Coninck, H. D., Gasda, S. E., Ghaleigh, N. S., Gooyert, V. D., Hajibeygi,
 396 H., ... Swennenhuis, F. (2023). Subsurface carbon dioxide and hydrogen stor-
 397 age for a sustainable energy future. *Nature Reviews Earth Environment* —, 4,
 398 102-118. doi: 10.1038/s43017-022-00376-8
- 399 Krevor, S., Pini, R., Li, B., & Benson, S. M. (2011). Capillary heterogeneity trap-
 400 ping of co₂ in a sandstone rock at reservoir conditions. *Geophysical Research*
 401 *Letters*, 38. doi: 10.1029/2011GL048239
- 402 Krishnamurthy, P. G., DiCarlo, D., & Meckel, T. (2022). Geologic heterogeneity
 403 controls on trapping and migration of co₂. *Geophysical Research Letters*, 49.
 404 doi: 10.1029/2022GL099104
- 405 Krishnamurthy, P. G., Meckel, T. A., & DiCarlo, D. (2019). Mimicking geologic de-
 406 positional fabrics for multiphase flow experiments. *Water Resources Research*,
 407 55, 9623-9638. doi: 10.1029/2019WR025664
- 408 Krishnamurthy, P. G., Senthilnathan, S., Yoon, H., Thomassen, D., Meckel, T., &
 409 DiCarlo, D. (2017). Comparison of darcy's law and invasion percolation sim-
 410 ulations with buoyancy-driven co₂-brine multiphase flow in a heterogeneous
 411 sandstone core. *Journal of Petroleum Science and Engineering*, 155, 54-62.
 412 doi: 10.1016/J.PETROL.2016.10.022
- 413 Kurotori, T., & Pini, R. (2021). A general capillary equilibrium model to describe
 414 drainage experiments in heterogeneous laboratory rock cores. *Advances in Wa-*
 415 *ter Resources*, 152. doi: 10.1016/j.advwatres.2021.103938
- 416 Li, B., & Benson, S. M. (2015). Influence of small-scale heterogeneity on upward co₂
 417 plume migration in storage aquifers. *Advances in Water Resources*, 83, 389-
 418 404. doi: 10.1016/j.advwatres.2015.07.010
- 419 Masalmeh, S. K. (2003). The effect of wettability heterogeneity on capillary pressure
 420 and relative permeability. *Journal of Petroleum Science and Engineering*, 39,
 421 399-408. doi: 10.1016/S0920-4105(03)00078-0
- 422 Mayer, A., & Miller, C. (1992). The influence of porous medium characteristics and
 423 measurement scale on pore-scale distributions of residual nonaqueous-phase
 424 liquids. *Journal of Contaminant Hydrology*, 11, 189-213.
- 425 Ni, H., Bakhshian, S., & Meckel, T. A. (2023). Effects of grain size and small-scale
 426 bedform architecture on co₂ saturation from buoyancy-driven flow. *Scientific*

- 427 *Reports*, 13. doi: 10.1038/s41598-023-29360-y
- 428 Ni, H., Boon, M., Garing, C., & Benson, S. M. (2019). Predicting co₂ residual
429 trapping ability based on experimental petrophysical properties for differ-
430 ent sandstone types. *International Journal of Greenhouse Gas Control*, 86,
431 158-176. doi: 10.1016/j.ijggc.2019.04.024
- 432 Ni, H., & Meckel, T. A. (2021). Characterizing the effect of capillary heterogeneity
433 on multiphase flow pulsation in an intermediate-scale beadpack experiment
434 using time series clustering and frequency analysis. *Water Resources Research*,
435 57. doi: 10.1029/2021WR030876
- 436 Niemet, M. R., Rockhold, M. L., Weisbrod, N., & Selker, J. S. (2002, 8). Relation-
437 ships between gas-liquid interfacial surface area, liquid saturation, and light
438 transmission in variably saturated porous media. *Water Resources Research*,
439 38, 10-1-10-12. doi: 10.1029/2001wr000785
- 440 Rubin, D. M., & Carter, C. L. (2006). *Cross-bedding, bedforms, and paleocurrents*
441 (Second ed., Vol. 1).
- 442 Seyyedi, M., Clennell, M. B., & Jackson, S. J. (2022). Time-lapse imaging of
443 flow instability and rock heterogeneity impacts on co₂ plume migration
444 in meter long sandstone cores. *Advances in Water Resources*, 164. doi:
445 10.1016/j.advwatres.2022.104216
- 446 Spiteri, E. J., Juanes, R., Blunt, M. J., & Orr, F. (2008). A new model of trap-
447 ping and relative permeability hysteresis for all wettability characteristics. *SPE*
448 *Journal*, 3, 277-288.
- 449 Tidwell, V. C., & Glass, R. J. (1994). X ray and visible light transmission for labo-
450 ratory measurement of two-dimensional saturation fields in thin-slab systems.
451 *Water Resources Research*, 30, 2873-2882. doi: 10.1029/94WR00953
- 452 Trevisan, L., Gonzalez-Nicolas, A., Cihan, A., Pini, R., Birkholzer, J., & Illan-
453 gasekare, T. (2017). Experimental and modeling study of capillary/buoyancy-
454 driven flow of surrogate co₂ through intermediate-scale sand tanks. *Energy*
455 *Procedia*, 114, 5032-5037. doi: 10.1016/J.EGYPRO.2017.03.1653
- 456 Trevisan, L., Pini, R., Cihan, A., Birkholzer, J. T., Zhou, Q., Gonzalez-Nicolas, A.,
457 & Illangasekare, T. H. (2017). Imaging and quantification of spreading and
458 trapping of carbon dioxide in saline aquifers using meter-scale laboratory ex-
459 periments. *Water Resources Research*, 485-582. doi: 10.1002/2016WR019749
- 460 Trevisan, L., Pini, R., Cihan, A., Birkholzer, J. T., Zhou, Q., & Illangasekare, T. H.
461 (2015, 11). Experimental analysis of spatial correlation effects on capillary
462 trapping of supercritical co₂ at the intermediate laboratory scale in het-
463 erogeneous porous media. *Water Resources Research*, 51, 8791-8805. doi:
464 10.1002/2015WR017440
- 465 Wang, S., & Tokunaga, T. K. (2015, 6). Capillary pressure-saturation relations
466 for supercritical co₂ and brine in limestone/dolomite sands: Implications for
467 geologic carbon sequestration in carbonate reservoirs. *Environmental Science*
468 *and Technology*, 49, 7208-7217. doi: 10.1021/acs.est.5b00826
- 469 Weisbrod, N., Niemet, M. R., & Selker, J. S. (2003, 8). Light transmission technique
470 for the evaluation of colloidal transport and dynamics in porous media. *Envi-*
471 *ronmental Science and Technology*, 37, 3694-3700. doi: 10.1021/es034010m